





Tracking the nuclear movement of the carbonyl sulfide cation after strong-field ionization by time-resolved Coulomb-explosion imaging

Xinning Zhao ¹, Ting Xu,² Xitao Yu,¹ Dianxiang Ren,¹ Xinyu Zhang,¹ Xiaokai Li,¹ Pan Ma,¹ Chuncheng Wang,¹ Dongdong Zhang ¹, Qinxin Wang,³ Xiaoqing Hu ^{2,*}, Sizuo Luo ^{1,†}, Yong Wu,² Jianguo Wang,² and Dajun Ding^{1,‡}

¹*Institute of Atomic and Molecular Physics, Jilin University, Changchun 130012, China*

²*Institute of Applied Physics and Computational Mathematics, Beijing 100088, China*

³*College of Electrical Engineering, Jilin Engineering Normal University, Changchun 130012, China*



(Received 15 March 2021; accepted 22 April 2021; published 5 May 2021; corrected 11 May 2021)

We studied the ultrafast nuclear dynamics during the dissociation of OCS^+ molecules using a strong IR-laser pump and probe technique in combination with the coincidence measurement. The nuclear movement is tracked by analyzing the time-dependent kinetic energy release (KER) spectra. The involved dissociation states and pathways are assigned with the help of the semiclassical Landau-Zener surface hopping calculations. The real-time bond-breaking dynamics of the $3^2A'$ coupling to other states are observed for the two-body dissociation channel and the three-body dissociation channel but with high KER. The three-body dissociation channel with low KER is assigned to the direct breaking process from the $3^2A''$ state. The overall agreements between the experimental and theoretical results demonstrate that the time-resolved Coulomb-explosion imaging is a valuable way to monitor the bond breaking and structural evolution of complex molecules.

DOI: [10.1103/PhysRevA.103.053103](https://doi.org/10.1103/PhysRevA.103.053103)

I. INTRODUCTION

The interaction of intense near-IR laser pulses with molecules will induce subsequent tunneling ionization [1,2], strong-field autoionization [3], high-harmonic generation [4,5], dissociation, and Coulomb explosion (CE) [6–8], where the inherent electron and nuclear dynamics is a subject of current interest. The coherent nuclear wave packets induced by the laser pulse evolve subsequently and lead to bond breaking, deformation, or rearrangement [9–15]. Tracking the nuclear movement after strong-field ionization not only provides insight into molecular dynamics on an ultrafast timescale but also, in many cases, allows extraction of the transient structures of molecules and the properties of the active potential energy surfaces (PESs), such as conical intersection and roaming of atoms or functional groups within a molecule [16,17]. Laser-induced Coulomb-explosion imaging shows its ability on determining the structure of molecules and clusters with picosecond to femtosecond resolution, which paves the way to the goal of real-time imaging of dynamical structures of complex molecular and cluster dissociation processes [12–16]. Nowadays, the bond length and geometry of molecules or clusters as well as the ultrafast evolution of conical intersection can be imaged [16]. The evolution of complex structures during roaming on PESs of a polyatomic molecule can be captured in real time [17]. Furthermore, the angstrom spatial resolution of time-resolved structural evolution on a subfemtosecond timescale can be achieved to fully understand the

ionization and dissociation mechanisms of molecules in ultrafast laser fields [8,18,19].

For carbonyl sulfide (OCS), an asymmetric triatomic molecule, the ionization, dissociation, and high-harmonic generation in strong laser fields have been extensively studied [12–25]. The ionization dynamics and the involved asymmetric molecular orbital have been tracked by measuring the photoelectron and photoion spectra [20–24]. The resonance enhanced ionization during bond breaking has been studied [26,27], the Coulombic and pre-Coulombic dissociation has been observed [26], and the concerted and sequential fragmentation processes during the three-body dissociation are tracked by varying the laser pulse duration [28]. Rajput *et al.* reported a clear separation between the concerted and sequential fragmentation channels by analyzing the three-body breaking in the native frame [29]. Ma *et al.* studied the bond-breakage-dependent dissociation and the contribution of electron recollision during CE in the linear and circular polarized laser fields [24,30]. Although the geometric configuration of the ground state of a neutral OCS molecule is linear with the electron configuration of $6\sigma^27\sigma^28\sigma^29\sigma^22\pi^43\pi^4$, the bending of the molecular ions after removing several electrons has been extensively discussed [26–28]. Even more, Zhao *et al.* successfully observed the bond rearrangement of OCS molecules after being ionized by strong laser fields [31]. However, fully understanding the evolution of a nuclear wave packet after strong-field ionization requires a time-resolved Coulomb-explosion imaging (CEI) measurement assisted by the high-quality PESs calculation and the nuclear movement simulation.

In this work, the femtosecond dissociation dynamics of OCS^+ cations is studied by performing the time-resolved CEI measurements and the semiclassical Landau-Zener surface

*hu_xiaoqing@iapcm.ac.cn

†luosz@jlu.edu.cn

‡dajund@jlu.edu.cn

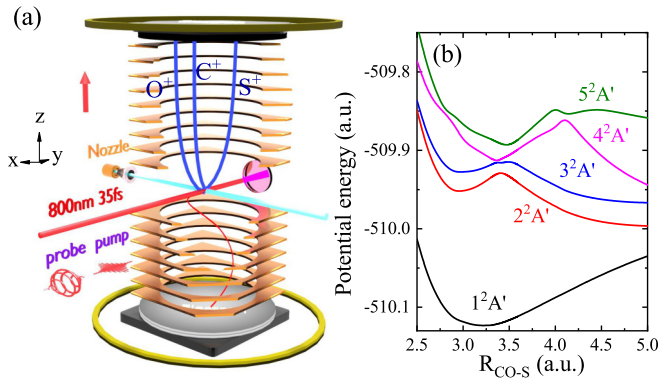


FIG. 1. (a) Schematic illustration of the experimental setup. (b) The calculated potential energy curves of OCS^+ with stretching the CO-S bond at $\theta_{\text{OCS}} = 165^\circ$.

hopping simulations. The nuclear movements along the PESs of singly charged OCS triggered by strong-field ionization are probed by a delayed strong laser pulse by performing coincidence measurements ($\text{OCS}^{3+} \rightarrow \text{CO}^+ + \text{S}^{2+}$, $\text{O}^+ + \text{C}^+ + \text{S}^+$) for channel identification. The semiclassical trajectory simulations can well reproduce the measured time-resolved kinetic energy release (KER) spectra of different channels, which further reveal the ultrafast bond-breaking dynamics related to coupling between cation states. The obtained overall good agreements between the experimental and theoretical results demonstrate that the time-resolved coincidence measurement is a valuable way to monitor the structural evolutions and extract the properties of the active PESs of molecules on the femtosecond timescale.

II. EXPERIMENTAL AND THEORETICAL METHODS

The measurements are performed in the cold-target recoil momentum spectrometer [32,33] and have been described in detail in our previous papers [12,34,35]. As shown in Fig. 1(a), a jet of OCS s enters an ultrahigh-vacuum chamber (along the y axis) and interacts with femtosecond laser pulses. The femtosecond laser pulses (800 nm, 1 kHz, ~ 35 fs) propagating along the x direction are focused onto the jet, and less than one molecule per laser shot is ionized during the experiment. The linearly polarized pump and circularly polarized probe lasers (1.0×10^{14} W/cm 2 , 4.0×10^{14} W/cm 2) are recombined after passing through a Mach-Zehnder interferometer and then are sent and focused into the reaction chamber. The intensity of the pumping laser is adjusted to ionize one electron from the OCS molecule. The probing laser further ionizes the other two electrons and populates the samples to trication states. The zero-time delay of two laser pulses is determined by measuring the time-dependent signal of parent ions. The full width at half maximum of the cross-correlation profile of two pulses is ~ 90 fs determined from a Gaussian fitting. The produced ions are extracted and projected to a time- and position-sensitive detector by a weak homogeneous electric field (16.9 V/cm). The mass-to-charge ratio and three-dimensional momentum distribution of the ions are calculated from the measured time and position information. To reduce the time jitter between two laser pulses

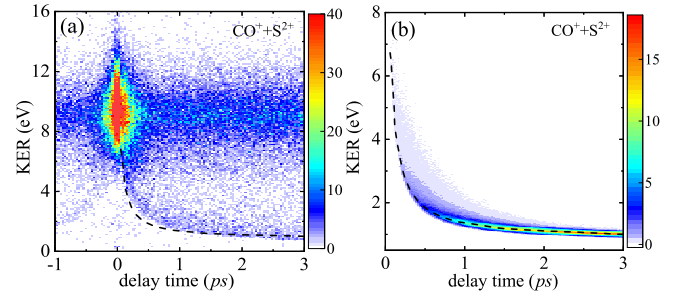


FIG. 2. (a) The measured time-dependent KER spectra of the two-body CE channel $\text{CO}^+ + \text{S}^{2+}$. (b) The calculated time-dependent KER spectra from further ionizing the OCS^+ to trication state by using the semiclassical Landau-Zener surface hopping method. The black dashed curve shown in (a) is adopted from (b) for comparing the evolutions between experiment and theory, and the curve is simply created by extracting the data from the simulation spectra.

during the long-term measurements, we scan the delay from -1 to 3 ps in steps of 33.3 fs every 10 min and repeat the scan until collecting enough data for further analysis.

In theory, we calculate the three-dimensional PESs of OCS^+ by the complete active space self-consistent field method [36–38], a combination of an SCF computation with a full configuration interaction involving a subset of the orbitals (known as the active space). Here, the active space is comprised of all valence orbitals ($2s2p$ for O and C; $3s3p$ for S) and all the states included in this active space are optimized simultaneously. The calculated potential energy curves of OCS^+ with stretching the CO-S bond at bending geometric configuration ($\theta_{\text{OCS}} = 165^\circ$) is shown in Fig. 1(b). Then, we simulate the two-body and three-body breakups of OCS^+ by using the semiclassical trajectory method [39]. In present simulations, the interactions among three particles C, O, and S are obtained by the derivative of the PES, and the fragment ions are treated as the point charges during the Coulomb-explosion process. $R_{\text{C-O}}$, $R_{\text{C-S}}$, and θ_{OCS} are initially set with Gaussian distributions with the widths of 0.15 a.u., 0.23 a.u., and 15° centered at the neutral equilibrium geometry. Once the particles move close to the avoided crossing position, the OCS^+ ions may transfer among different electronic states. The transfers among four ${}^2A'$ states (${}^2A' - {}^5^2A'$) and two ${}^2A''$ states (${}^3^2A'' - {}^4^2A''$) are included in our calculations and the transfer rates are calculated by Landau-Zener theory. The final KER spectra are obtained by projecting the real-time nuclear geometry of molecules during the evolutions among PESs to the trication states, where the KER is accumulated from the repelling energies between charged spaces during two-body ($\text{OCS}^{3+} \rightarrow \text{CO}^+ + \text{S}^{2+}$) and three-body ($\text{OCS}^{3+} \rightarrow \text{O}^+ + \text{C}^+ + \text{S}^+$) dissociation from trication Coulomb repulsive states.

III. RESULTS AND DISCUSSION

The measured time-dependent KER spectra from the two-body CE channel, $\text{OCS}^{3+} \rightarrow \text{CO}^+ + \text{S}^{2+}$, is shown in Fig. 2(a), which splits into two branches at positive delay time. For the negative delay, the pump and probe pulses reverse roles on

inducing and probing the dynamics of molecular cation states, while the time-dependent KER spectra are mirroring with the positive delay since two pulses perform a similar contribution. The KER around 9 eV remains unchanged as the delay time increases and the signal from this branch is generated from direct CE of OCS^{3+} . The observed KER distribution for this branch is in good agreement with previously reported results for strong-field-induced CE of OCS [24]. However, the KER of the other branch decreases gradually as the delay time increases and reaches the asymptotic energies (~ 1 eV) at the delay time of 3 ps. Since the KER from CE depends on the transient structures, i.e., the relative position of atoms in the molecules, the decrease of the KER value corresponds to the bond breaking of molecules. This dissociative two-body channel is reproduced by performing the molecular dynamics simulations based on the semiclassical Landau-Zener surface hopping method on the PES of the cation, and the results are given in Fig. 2(b). Four cation states ($2-5^2A'$) are taken into account, and the initial conditions are sampled at $2^2A'$ and $3^2A'$ states. The nuclear wave function of molecules is evaluated in the full three-dimensional PESs of these four states. The simulated KER decreases from around 7 eV at 0 ps to 1 eV at 3 ps; both the transient evolution and the asymptotic energies agree well with the experiments as illustrated by the black dashed curves. This agreement indicates that the two-body breakup process can be assigned as the dissociation of the $3^2A'$ state, which has a lower potential barrier. Furthermore, we point out that the products $\text{CO} + \text{S}^+$ are mainly generated by the coupling between $3^2A'$ and $5^2A'$ states from analyzing the trajectories hopped between these PESs.

For three-body channel $\text{OCS}^{3+} \rightarrow \text{C}^+ + \text{O}^+ + \text{S}^+$ there are three noticeable KER branches. The measured time-dependent KER spectra are shown in Fig. 3(a). One branch with the KER peak around 16.5 eV, which remains unchanged as the delay time increases. The measured value is consistent with that obtained from the direct three-body CE of OCS^{3+} [28–30]. For the other two branches, the KER decreases as the delay time increases, which indicates that two dissociative states are responsible for these two channels [10–12]. The higher one reaches the asymptotic energies around 6.3 eV and the lower one has the asymptotic energies ~ 1.2 eV. The integral KER spectra at different delay times (0.3, 0.5, and 1.0 ps) are presented in Fig. 3(b). It is worth noting that the KER spectrum with energy below 11 eV has only one peak at 0.3 ps, while the spectra become two-peak distributions when the delay time reaches 0.5 and 1.0 ps. Therefore, we can further analyze the dissociation dynamics by selecting the data from these two channels at the delay time above 0.5 ps. Generally speaking, the three-body CE ($\text{C}^+ + \text{O}^+ + \text{S}^+$) can occur from two distinguishable pathways, the direct and the sequential pathways [28,29,40]. The direct pathway occurs as direct three-body fragmentation after the interaction with the pumping laser. The released two neutral fragments get further ionized by the probing laser in this case. The other is the sequential pathway in which the pumping laser firstly triggers a two-body dissociation, and then a further fragmentation of the metastable intermediate is induced by the probing laser.

The total KER from the time-resolved measurement equals the summation of the energy release (E_0) during the dissocia-

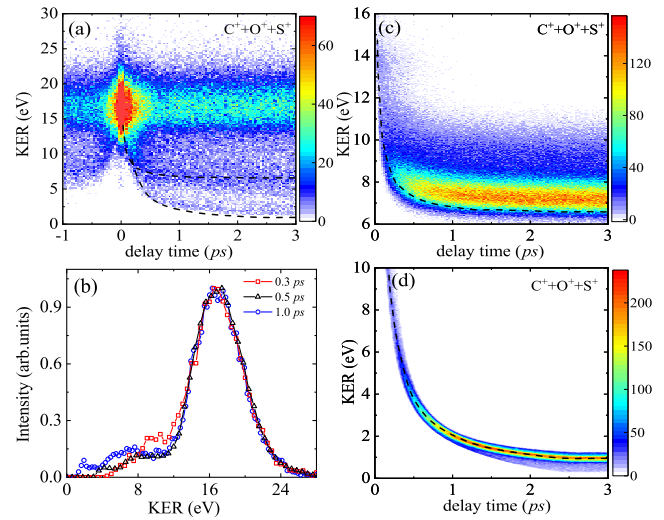
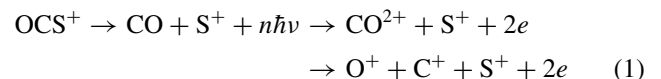
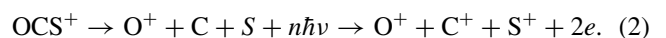


FIG. 3. (a) The measured time-dependent KER for the three-body CE channel $\text{C}^+ + \text{O}^+ + \text{S}^+$. (b) The integral KER spectra at three delay times (0.3, 0.5, and 1.0 ps) between pump-probe lasers. (c) and (d) are the calculated time-dependent KER from sequential dissociation pathway and direct three-body fragmentation pathway. The black dashed curves shown in (a) are adopted from (b) and (c) for comparing the evolutions between experiment and theory, and the curves are simply created by extracting the data from the simulation spectra.

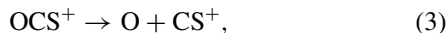
tion process triggered by the pumping laser and the following Coulomb energy (E_{Coulb}) accumulated from repelling between three ions by the probing laser, i.e., $\text{KER} = E_0 + E_{\text{Coulb}}$. Thus, different pathways will accumulate different final asymptotic KER after the further CE process followed by the dissociation of the OCS^+ . The direct three-body fragmentation has a smaller final KER since three pieces are far away from each other when CE occurs. On the other hand, the ions from the sequential pathway have larger final kinetic energies because the CE of metastable molecular ions leads to a high Coulomb repelling energy. Thus, the asymptotic energy is a characteristic value to determine the dissociative channels. Here, the channel with high final asymptotic energy can be assigned to the sequential dissociation pathway, in which the two-body dissociation of OCS^+ occurs, and produces $\text{CO} + \text{S}^+$ after strong-field ionization by the pumping laser. The further double ionization of CO by the probing laser leads to the subsequent CE of $\text{CO}^{2+} \rightarrow \text{C}^+ + \text{O}^+$. The measured asymptotic energy ~ 6.3 eV of this channel is attributed to the sum energy of the first dissociation process and the second CE process of CO^{2+} [35]. The low KER channel can be assigned to the direct three-body fragmentation of OCS^+ with products of $\text{O}^+ + \text{C} + \text{S}$, which accumulates a lower final asymptotic energy. To summarize, the sequential pathway is given in



and the direct pathway is written as



In order to further investigate the ultrafast nuclear dynamics during the three-body dissociation of OCS molecules, semiclassical trajectory simulations are performed. The simulated time-dependent KER spectra of three-body CE channels from these two pathways are given in Figs. 3(c) and 3(d), from where the evolutions agree with the measured transient behaviors for both high and low dissociative branches as marked by two black dashed curves in Fig. 3(a). Notably, the simulation reproduces the same asymptotic energies as obtained from measurements. Both simulations are carried out for the cation states, but the underlying mechanism is quite different. Theoretically, the sequential and direct fragmentation channels can be assigned by comparing the holding time of intermediate products with the rotational period of products. In the sequential pathways, the holding time is comparable or longer than the rotational period, while the holding time should be much shorter than the rotational period for the direct breaking pathway. The high KER channel is assigned to the sequential channel, for which the dissociation mainly starts in the $3^2 A'$ state, and crosses the $4^2 A'$ and $5^2 A'$ states by orbital overlapping and conical intersection leading to the final dissociation. The OCS^+ firstly breaks into $\text{CO} + \text{S}^+$ in the same way as the ultrafast nuclear evolution of the two-body channel as previously discussed. These two fragments are further ionized to produce CO^{2+} and S^+ by the probing laser, then, the CO^{2+} is further breaking into C^+ and O^+ after a long delay time. In the present simulation, the full three-dimensional rotation of CO^{2+} is considered with the lifetime set as 10 ps [29] and the total propagation time is 100 ps. In addition to the rotation caused by releasing an S^+ , the random rotation of the molecule at the temperature condition of our experiment is also considered. The total asymptotic energy for this pathway equals the sum of the KER for the $\text{OCS}^+ \rightarrow \text{CO} + \text{S}^+$ channel and the $\text{CO}^{2+} \rightarrow \text{O}^+ + \text{C}^+$ channel, and the value is around 7.2 eV derived from our calculation. The simulation of the low KER channel is performed by assuming a short holding time of intermediate product instead of performing the direct three-body dissociation simulations. We simplify it to a stepwise breaking process with the first step following



while within the pumping laser the CS^+ is further excited to the direct dissociative state by absorbing two or three photons and then dissociates following



Then, the neutral atoms O and C are ionized to O^+ and C^+ by the probing laser. For the simulation of the low KER channel, the OCS^+ ion is located at the $3^2 A''$ state firstly and then transfers to the $2^2 A''$ state by radial coupling. Since the coupling is very strong—the transfer probability is larger than 90%—the dissociations of the OCS^+ ion from the $3^2 A''$ state can be treated as a direct breakup process. Furthermore, after the pump laser is over, we suppose that the CS^+ ion has been excited to a direct dissociative state $^2 \Delta$ and dissociates along with the repulsive PES. Finally, the kinetic energies of three particles can be obtained and the time-dependent KER spectra are shown in Fig. 3(d). The overall agreement between theory and experiment confirms that the direct breakup mechanism

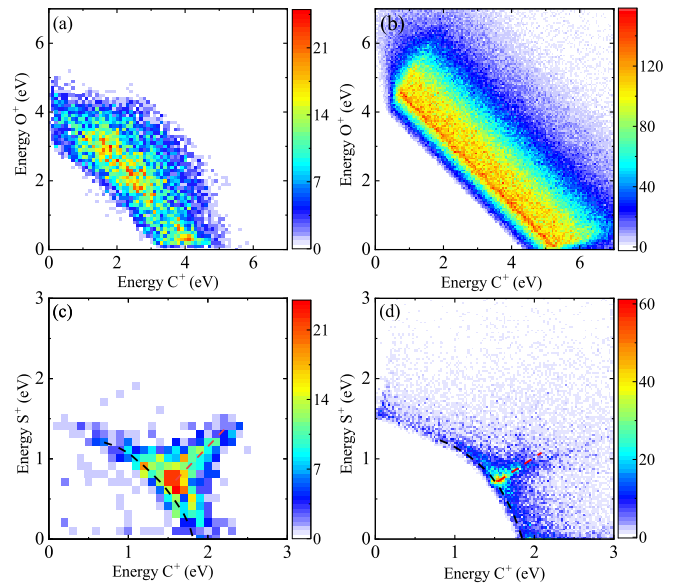


FIG. 4. (a) and (b) are the measured and calculated kinetic energy correlation diagrams for the C^+ and O^+ ions from the high KER channel at a delay time of 0.5 ps. (c) and (d) are the measured and calculated kinetic energy correlation diagrams between the C^+ and S^+ ions from the low KER channel at a delay time of 0.5 ps. The black dashed curves and the red dashed lines are marked to present the two different correlations between fragments.

of the OCS^+ ion is indeed consistent with our experimental results.

The energy sharing and correlations between fragments are different for sequential and direct breaking pathways [12,41]. Thus, in order to further confirm the above conclusion on the three-body dissociation process, the measured and calculated kinetic energy correlations between fragments at a delay time of 0.5 ps are shown in Fig. 4. We chose a delay time of 0.5 ps because here the KER is distinctively different in the two channels as shown in Fig. 3(b). Choosing this delay, we can further analyze and compare the correlations between the fragments after selecting the data within the KER ranges of 1–4 eV and 5–7.5 eV. In the sequential dissociation pathway where the KER is higher, the C and O do not separate before further ionization. Thus, C^+ and O^+ share the same total energy from the breaking of intermediate products CO^{2+} , and this assumption is confirmed by the measured and calculated energy sharing between C^+ and O^+ as shown in Figs. 4(a) and 4(b). The agreement between the kinetic energy correlation maps further demonstrates the high KER channel is generated from sequential fragmentation pathways, and the difference in their sum energy, i.e., 4.2 eV from an experiment comparing to around 5 eV from theory, may be generated from the overestimates of the bond stretching and the underestimates of vibration excitation during strong-field ionization of molecules in simulation. There is also a noticeable asymmetry energy correlation between C^+ and O^+ as shown in Fig. 4(a), which can be assigned to the rotation of CO induced by the imparted recoil momentum of the S^+ atom during the dissociation at a short delay time. The absence of asymmetry in the simulation can be assigned as the overestimates of the

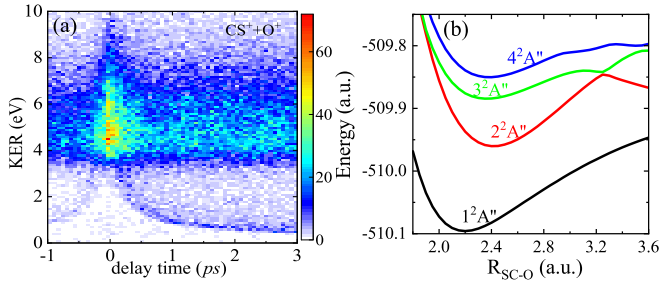


FIG. 5. (a) The measured time-dependent KER spectra of the $O^+ + CS^+$ channel. (b) is the potential energy curves of OCS^+ corresponding to the bond stretching between the O and C atoms.

bond stretching of $CO-S^+$ and the lifetime of CO^{2+} . However, the correlation between C^+ and S^+ of the low KER channel from three-body breaking shows quite different distribution as presented in Figs. 4(c) and 4(d). The correlation map can be simply divided into two parts: one with the correlation sharing the energy which is also influenced by the third fragments as marked by the black dashed curves, and the other part without energy correlation which is generated from a direct three-body breaking pathway as marked by the red dashed lines. These two parts are both observed in the theoretical simulation and present the same distribution with the measured map. By tracking the dissociation trajectories, we find that the molecules break up immediately when they first reach the avoided crossing position for the signals marked in the red dashed lines, and the molecular dissociation occurs after one or several vibrational periods with a rapid bending in θ_{OCS} for those signals as illustrated by the black dashed curves.

The agreement between theoretical calculations and experimental measurements indicates that the low KER channel of the three-body CE can be assigned as the step dissociation with $O + CS^+$ produced in the first step. Furthermore, this can be checked again by comparing the time-dependent KER of the three-body channel (low KER) with the spectra obtained from the two-body dissociation $O^+ + CS^+$. The measured time-dependent KER of $O^+ + CS^+$ is shown in Fig. 5(a),

where two branches corresponding to the direct CE of dication states and the CE by further ionization from cation states are observed. The time-dependent branch can be assigned to the CE followed by the dissociation of the $3^2A''$ state, and the corresponding potential energy curves are shown in Fig. 5(b). The observation for the evolution of the $O^+ + CS^+$ channel presents additional evidence on the assignment of the pathway of the direct three-body CE channel.

IV. CONCLUSIONS

We have performed the pump-probe measurements to tracking the bond breaking of OCS^+ triggered by an femtosecond laser. The time-dependent KER spectra of two-body and three-body channels are measured and the corresponding electronic states and dissociation pathways are assigned by comparing the simulation results from performing the semi-classical trajectory simulations. The two-body dissociation channel and the three-body dissociation channel with high KER are assigned to the bond breaking started from the $3^2A'$ state and the following couplings with other electronic states are analyzed from the trajectories of nuclear movement. Furthermore, the three-body dissociation channel with low KER is assigned to the direct three-body breaking process after populated to the $3^2A''$ state. The assignments of the bond breaking of three-body channels are further confirmed by the measured and calculated kinetic energy correlation diagrams of fragment ions. Thus, the current study paves the way for tracking the bond breaking and structural evolution of molecules and promotes our understanding of the elementary reaction and light-induced molecular process.

ACKNOWLEDGMENTS

This work was supported by the National Basic Research Program of China (Grant No. 2019YFA0307700), the National Natural Science Foundation of China (Grants No. 12074143, No. 12004135, No. 11934004, and No. 11627807), and Science Challenge Project No. TZ2018005.

X.Z. and T.X. contributed equally to this work.

- [1] U. S. Sainadh, H. Xu, X. Wang, A. Atia-Tul-Noo, W. C. Wallace, N. Douguet, A. Bray, I. Ivanov, K. Bartschat, A. Kheifets, R. T. Sang, and I. V. Litvinyuk, *Nature (London)* **568**, 75 (2019).
- [2] W. Quan, V. V. Serov, M. Z. Wei, M. Zhao, Y. Zhou, Y. L. Wang, X. Y. Lai, A. S. Kheifets, and X. J. Liu, *Phys. Rev. Lett.* **123**, 223204 (2019).
- [3] S. Luo, J. Liu, X. Li, D. Zhang, X. Yu, D. Ren, M. Li, Y. Yang, Z. Wang, P. Ma, C. Wang, J. Zhao, Z. Zhao, and D. Ding, *Phys. Rev. Lett.* **126**, 103202 (2021).
- [4] M. Lewenstein, P. Balcou, M. Y. Ivanov, A. L'Huillier, and P. B. Corkum, *Phys. Rev. A* **49**, 2117 (1994).
- [5] C. Winterfeldt, C. Spielmann, and G. Gerber, *Rev. Mod. Phys.* **80**, 117 (2008).
- [6] V. Hanus, S. Kangaparambil, S. Larimian, M. Dorner-Kirchner, X. Xie, M. S. Schöffler, G. G. Paulus, A. Baltuška, A. Staudte, and M. Kitzler-Zeiler, *Phys. Rev. Lett.* **123**, 263201 (2019).
- [7] Q. Ji, S. Pan, P. He, J. Wang, P. Lu, H. Li, X. Gong, K. Lin, W. Zhang, J. Ma, H. Li, C. Duan, P. Liu, Y. Bai, R. Li, F. He, and J. Wu, *Phys. Rev. Lett.* **123**, 233202 (2019).
- [8] V. Hanus, S. Kangaparambil, S. Larimian, M. Dorner-Kirchner, X. Xie, M. S. Schöffler, G. G. Paulus, A. Baltuška, A. Staudte, and M. Kitzler-Zeiler, *Phys. Rev. Lett.* **124**, 103201 (2020).
- [9] T. Ergler, A. Rudenko, B. Feuerstein, K. Zrost, C. D. Schröter, R. Moshhammer, and J. Ullrich, *Phys. Rev. Lett.* **97**, 193001 (2006).
- [10] S. De, M. Magrakvelidze, I. A. Bocharova, D. Ray, W. Cao, I. Znakovskaya, H. Li, Z. Wang, G. Laurent, U. Thumm, M. F. Kling, I. V. Litvinyuk, I. Ben-Itzhak, and C. L. Cocke, *Phys. Rev. A* **84**, 043410 (2011).
- [11] I. A. Bocharova, A. S. Alnaser, U. Thumm, T. Niederhausen, D. Ray, C. L. Cocke, and I. V. Litvinyuk, *Phys. Rev. A* **83**, 013417 (2011).

- [12] X. Zhao, X. Yu, X. Xu, Z. Yin, J. Yu, X. Li, P. Ma, D. Zhang, C. Wang, S. Luo, and D. Ding, *Phys. Rev. A* **101**, 013416 (2020).
- [13] N. G. Kling, S. D. Tendero, R. Obaid, M. R. Disla, H. Xiong, M. Sundberg, S. D. Khosravi, M. Davino, P. Drach, A. M. Carroll, T. Osipov, F. Marín, and N. Berrah, *Nat. Commun.* **10**, 2813 (2019).
- [14] K. Lin, X. Hu, S. Pan, F. Chen, Q. Ji, W. Zhang, H. Li, J. Qiang, F. Sun, X. Gong, H. Li, P. Lu, J. Wang, Y. Wu, and J. Wu, *J. Phys. Chem. Lett.* **11**, 3129 (2020).
- [15] M. McDonnell, A. C. LaForge, J. Reino-González, M. Disla, N. G. Kling, D. Mishra, R. Obaid, M. Sundberg, V. Svoboda, S. Díaz-Tendero, F. Martín, and N. Berrah, *J. Phys. Chem. Lett.* **11**, 16, 6724 (2020).
- [16] M. E. Corrales, J. González-Vázquez, R. de Nalda, and L. Bañares, *J. Phys. Chem. Lett.* **10**, 138 (2019).
- [17] T. Endo, S. P. Neville, V. Wanie, S. Beaulieu, C. Qu, J. Deschamp, P. Lassonde, B. E. Schmidt, H. Fujise, M. Fushitani, A. Hishikawa, P. L. Houston, J. M. Bowman, M. S. Schuurman, F. Légaré, and H. Ibrahim, *Science* **370**, 1072 (2020).
- [18] S. Zeller, M. Kunitski, J. Voigtsberger, M. Waitz, F. Trinter, S. Eckart, A. Kalinin, A. Czasch, L. P. H. Schmidt, T. Weber, M. Schöffler, T. Jahnke, and R. Dörner, *Phys. Rev. Lett.* **121**, 083002 (2018).
- [19] A. Khan, T. Jahnke, S. Zeller, F. Trinter, M. Schöffler, L. H. Schmidt, R. Dörner, and M. Kunitski, *J. Phys. Chem. Lett.* **11**, 2457 (2020).
- [20] L. Holmegaard, J. L. Hansen, L. Kålhøj, S. L. Kragh, H. Stapelfeldt, F. Filsinger, J. Küpper, G. Meijer, D. Dimitrovski, M. Abu-samaha, C. P. J. Martiny, and L. B. Madsen, *Nat. Phys.* **6**, 428 (2010).
- [21] J. L. Hansen, L. Holmegaard, J. H. Nielsen, H. Stapelfeldt, D. Dimitrovski, and L. B. Madsen, *J. Phys. B* **45**, 015101 (2011).
- [22] J. Yu, W. Hu, X. Li, P. Ma, L. He, F. Liu, C. Wang, S. Luo, and D. Ding, *J. Phys. B* **50**, 235602 (2017).
- [23] Y. Sakemi, S. Minemoto, and H. Sakai, *Phys. Rev. A* **96**, 011401(R) (2017).
- [24] P. Ma, C. Wang, S. Luo, X. Li, W. Hu, J. Yu, X. Yu, X. Tian, Z. Qu, and D. Ding, *Phys. Rev. A* **99**, 023423 (2019).
- [25] P. M. Kraus, A. Rupenyan, and H. J. Wörner, *Phys. Rev. Lett.* **109**, 233903 (2012).
- [26] J. H. Sanderson, T. R. J. Goodworth, A. El-Zein, W. A. Bryan, W. R. Newell, A. J. Langley, and P. F. Taday, *Phys. Rev. A* **65**, 043403 (2002).
- [27] W. A. Bryan, W. R. Newell, J. H. Sanderson, and A. J. Langley, *Phys. Rev. A* **74**, 053409 (2006).
- [28] B. Wales, É. Isson, R. Karimi, S. Beaulieu, A. Ramadhan, M. Giguère, Z. Long, W. Liu, J. Kieffer, F. Légaré, and J. Sanderson, *J. Electron Spectrosc. Relat. Phenom.* **195**, 332 (2014).
- [29] J. Rajput, T. Severt, B. Berry, B. Jochim, P. Feizollah, B. Kaderiya, M. Zohrabi, U. Ablikim, F. Ziaee, K. Raju P., D. Rolles, A. Rudenko, K. D. Carnes, B. D. Esry, and I. Ben-Itzhak, *Phys. Rev. Lett.* **120**, 103001 (2018).
- [30] P. Ma, C. Wang, S. Luo, X. Yu, X. Li, Z. Wang, W. Hu, J. Yu, Y. Yang, X. Tian, Z. Cui, and D. Ding, *J. Phys. B* **51**, 094002 (2018).
- [31] S. Zhao, B. Jochim, P. Feizollah, J. Rajput, F. Ziaee, Kanaka Raju P., B. Kaderiya, K. Borne, Y. Malakar, B. Berry, J. Harrington, D. Rolles, A. Rudenko, K. D. Carnes, E. Wells, I. Ben-Itzhak, and T. Severt, *Phys. Rev. A* **99**, 053412 (2019).
- [32] R. Dörner, V. Mergel, O. Jagutzki, L. Spielberger, J. Ullrich, R. Moshhammer, and H. Schmidt-Böcking, *Phys. Rep.* **330**, 95 (2000).
- [33] J. Ullrich, R. Moshhammer, A. Dorn, R. Dörner, L. P. H. Schmidt, and H. Schmidt-Böcking, *Rep. Prog. Phys.* **66**, 1463 (2003).
- [34] C. Wang, X. Li, X. R. Xiao, Y. Yang, S. Luo, X. Yu, X. Xu, L. Y. Peng, Q. Gong, and D. Ding, *Phys. Rev. Lett.* **122**, 013203 (2019).
- [35] X. Li, J. Yu, H. Xu, X. Yu, Y. Yang, Z. Wang, P. Ma, C. Wang, F. Guo, Y. Yang, S. Luo, and D. Ding, *Phys. Rev. A* **100**, 013415 (2019).
- [36] H. J. Werner, P. J. Knowles, G. Knizia, F. R. Manby, M. Schütz, P. Celani, T. Korona, R. Lindh, A. Mitrushechkov, G. Rauhut *et al.*, MOLPRO, a package of *ab initio* programs, version 2010.1, <http://www.molpro.net>.
- [37] P. J. Knowles and H. J. Werner, *Chem. Phys. Lett.* **115**, 259 (1985).
- [38] H. J. Werner, P. J. Knowles, G. Knizia, F. R. Manby, and M. Schütz, *WIREs Comput. Mol. Sci.* **2**, 242 (2012).
- [39] A. K. Belyaev, W. Domcke, C. Lasser, and G. Trigila, *J. Chem. Phys.* **142**, 104307 (2015).
- [40] X. Q. Hu, Y. G. Peng, X. L. Zhu, S. C. Yan, L. Liu, W. T. Feng, D. L. Guo, Y. Gao, S. F. Zhang, D. M. Zhao, D. P. Dong, B. Hai, J. W. Xu, S. B. Zhang, X. Ma, J. G. Wang, and Y. Wu, *Phys. Rev. A* **101**, 012707 (2020).
- [41] C. Wu, C. Wu, D. Song, H. Su, Y. Yang, Z. Wu, X. Liu, H. Liu, M. Li, Y. Deng, Y. Liu, L. Y. Peng, H. Jiang, and Q. Gong, *Phys. Rev. Lett.* **110**, 103601 (2013).

Correction: The previously published Figure 3(d) was processed improperly during the production cycle and is now rendered correctly.